



## PROBABILISTIC RESILIENCE-BASED FRAMEWORK FOR ASSESSING TIME-DEPENDENT FUNCTIONALITY OF TALL BUILDINGS

X. Xiong<sup>(1)</sup>, H. Burton<sup>(2)</sup>, X. Lu<sup>(3)</sup>, Y. Zhang<sup>(4)</sup>

<sup>(1)</sup> Graduate Student Researcher, Department of Disaster Mitigation for Structures, Tongji University, Shanghai, [xxl\\_sunshine@tongji.edu.cn](mailto:xxl_sunshine@tongji.edu.cn)

<sup>(2)</sup> Assistant Professor, Department of Civil and Environmental Engineering University of California, Los Angeles, [hvburton@ucla.edu](mailto:hvburton@ucla.edu)

<sup>(3)</sup> Professor, State Key Laboratory of Disaster Reduction in Civil Engineering, Tongji University, Shanghai, [xlst@tongji.edu.cn](mailto:xlst@tongji.edu.cn)

<sup>(4)</sup> Graduate Student Researcher, Department of Civil and Environmental Engineering, University of California, Los Angeles, [y.zhang@ucla.edu](mailto:y.zhang@ucla.edu)

### Abstract

A probabilistic framework is introduced to assess the resilience of tall buildings in terms of time-dependent functionality following an earthquake event. The proposed methodology integrates component-level damage simulation, building-level post-event performance evaluation and story-level functionality restoration. Seismic demands and induced component damage is used to estimate repair workload and assess building performance limit states which are explicitly related to recovery activities. The building functionality as quantified by the number of serviceable stories is defined to specifically characterize the resilience of tall buildings. The functionality recovery event of each story is determined through reliability-wise configuration of unsafe-placard triggering components, common nonstructural components and vital mechanical equipment within the damaged building. State-based arrival process that accounts for utility disruption and resourcefulness constraints is developed on the relationship between the consumed recovery time and the number of functionality-restored stories. Genetic algorithm using hierarchical non-dominated sorting is employed to perform a multi-objective optimization and determine the optimal damage-repair workflow schedule. The recovery arrival time of each story is estimated on the optimized workflow schedule, and the arrival epoch is calculated as the order statistic of the recovery arrival series. The counting process of the arrivals is used to quantitatively delineate story functionality restoration over timeline. A case study is presented in which the proposed framework is applied to a 40-story steel moment resisting frame office building. Expected time-dependent functionality curves are plotted across multiple intensities ranging from 2% to 200% Sa of MCE levels. Functionality disruption during the recovery period is calculated as a measure of resilience. Loss of utility service outweighs preparative and repair activities in the influence of building resilience at extra-low intensities, while at higher intensities, the sharply-increased probability of building replacement makes the functionality disruption get close to the sum of the time consumed in engineering preparation and reconstruction. As a building-specific method, the framework presented in this paper provides an insight into the variation of functionality disruption across multiple ground intensities and can be used to guide the design practices to meet the resilience-based objectives.

*Keywords: resilience-based assessment; recovery process modeling; time-dependent functionality; system reliability*



## 1. Introduction

Post-earthquake functional state of hazard-damaged tall buildings during recovery process can inform socioeconomic impact of these commercial towers in central business district (CBD) and guide decision-making of occupants, owners and policymakers on ameliorative interventions which aim at improving emergency preparedness and response efficacy. All these efforts enable the stakeholders to contain the hazard effects and achieve a timely recovery which can be conceptualized as increasing the seismic resilience of their properties. Therefore, it is a reasonable point that the resilience of tall buildings can be interpreted from the restoration of their functionality after the hazard. Numerous prior studies focused on directly evaluating the resilience of impacted buildings in terms of the measurement like total repair (or reconstruction) cost and potential casualties [1-5]. However, increasingly more efforts [6-9] have been devoted to establishing resilience-based performance standards incorporating time-dependent functionality metric (i.e., quantitative vital building occupancy during a typical period following a natural hazard event), mainly because of the growing recognition that time-varying building functionality can provide a more complete understanding of the recovery process and be ideally set as resilience-based performance objective in future building design and community planning [10].

Endeavors to model disaster recovery process could be generally grouped into two main categories, empirical data-driven (EDD) and scenario simulation-based (SSB). Though most early researches are empirical data-driven [11-13], the relative scarcity of longitudinal data and the insufficient generalizability of event-specific model highlight the significance that computational techniques are needed to augment the EDD methods for further theoretical establishment and practical application [14]. Generally, SSB models, appropriately characterizing the contribution of hazard events, can leverage conceptual understanding of post-event restoration and relieve the reliance on collected event data in prediction of recovery process. Miles and Chang [15-16] presented a stochastic simulation model of community recovery called ResilUS, in which a Markov chain Monte Carlo (MCMC) approach was implemented. Burton et al. [17] proposed a time-based probabilistic approach in the assessment of residential community recovery incorporating post-earthquake building performance. A similar stochastic method was presented by Zhang et al. [18], in which multilevel Monte Carlo simulation was used to obtain the building portfolio functionality loss.

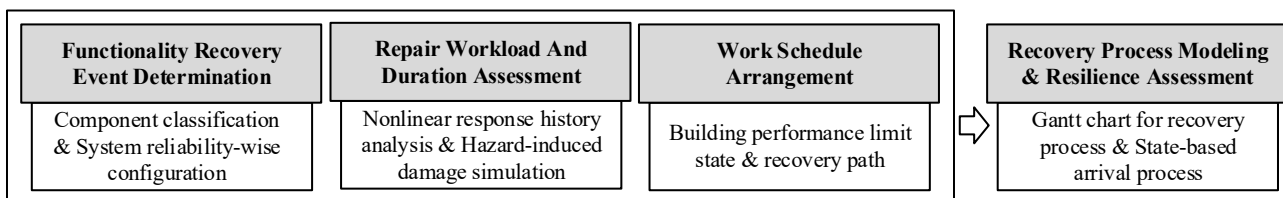


Fig. 1 – Overview of the resilience-based assessment framework

A building-specific SSB method is presented in this study. In attempts to estimate the time-dependent functionality of hazard-impacted buildings, the proposed resilience-based framework conducts the building recovery process modeling with a triple-module procedure, as illustrated in Fig.1. The first module is to determine functionality recovery event for each story in a damaged building based on component classification and building system reliability-wise configuration. Then, Nonlinear response history analysis (NRHA) is performed to obtain the engineering demand parameters (EDPs) at given intensity levels of ground motion. The approach of hazard-induced damage simulation implemented in FEMA P-58([19-21]) is adopted in assessing the repair workload and duration resulted from the structural deformation. Additionally, building performance limit states proposed by Burton et al [17] are introduced and correlated to those specific event routines of recovery activities, termed as recovery paths. Hence, the work schedule of the recovery process can be arranged and depicted by a Gantt Chart for each possible limit state according to the associated recovery path. On basis of the chronological order and duration of functionality recovery events, the recovery process is stochastically modeled as a state-based arrival process in this study. More details on recovery process modeling are provided in Section 2. The resourcefulness constraint and off-site impediment represented by maximum number of workers and utilities disruption are also considered in this methodology,



and a case study (a 40-story steel moment resisting frame office building) is shown to illustrate the resilience-based assessment in terms of functionality disruption using the proposed framework.

## 2. Development of building recovery process modeling

### 2.1 Functionality recovery event determination

A system reliability model is conceived and used to determine the story functionality restoration event based on the performance of building systems (e.g., structure, MEP and interior). Building components and assemblies within various systems are grouped into three performance categories (PC): unsafe-placard triggering components (UTC), common nonstructural components (CNC) and vital mechanical equipment (VME). UTC contain all the structural components and some nonstructural components relating to life-safety (e.g., fire sprinklers and suspended ceiling systems). CNC includes all the rest of nonstructural components (e.g., partitions, HAVC conducts, etc.), and VME are those powered devices or machineries facilitating building normal operation, like elevators and cooling towers. Fig.2 shows the system reliability-wise configuration of a typical tall building in CBD. UTC blocks represent the overall performance of UTC on a specific story, and UTC block fails when the severity of damage and the number of damaged components trigger the unsafe placard. UTC blocks are joined in series on the fact that building closure prompted by the failure of any UTC block can give rise to complete building functionality disruption and hinder the restoration for any part of building. VME blocks, which denote the accessibility and serviceability of mechanical floors, are linked in series because of their indispensable roles in building daily function. CNC blocks are in parallel based on the assumption that serviceability at an individual story may not be affected by damage to CNC on any other floors and story functionality can be achieved independently. Besides, off-site facility service (OFS) block which represents the vital utilities (e.g., electricity, water) provided by the supporting infrastructure is also considered and serially linked. From leftmost node to rightmost node of Fig.2, a minimum path set of the RBD can be used to describe an event that the function of an individual story is restored as follows,

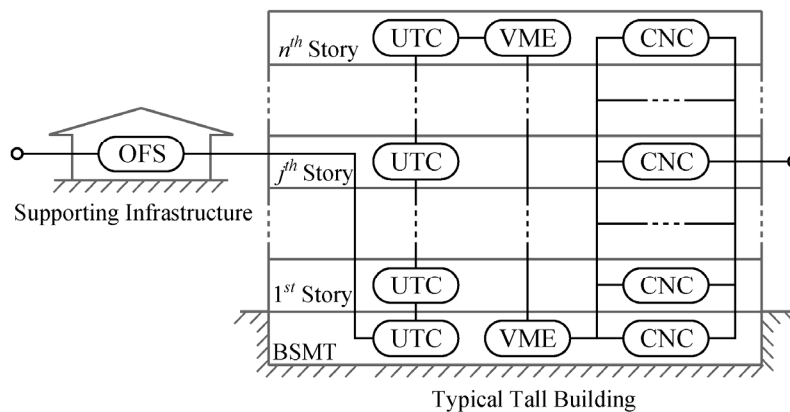


Fig. 2 –Reliability block diagram (RBD) of a typical tall building in CBD

$$E^{indv} = E_{OFS} \left( \bigcap_{j=1}^n E_{UTC}^j \right) \bigcap E_{CNC}^{indv} \bigcap E_{VME} \quad (1)$$

where  $E^{indv}$  represents the event that the functionality of an individual story is restored;  $E_{OFS}$  is the recovery subevent that all the OFS are restored;  $E_{VME}$  is the recovery subevent that VME are repaired and the mechanical floors are safe and accessible;  $E_{CNC}^{indv}$  represents the recovery subevent that repairs of CNC on the target story are complete;  $E_{UTC}^j$  represents the recovery subevent that repairs of UTC on the  $j^{\text{th}}$  story are complete, and  $n$  is the total number of the stories.

### 2.2 Repair workload and duration assessment



As stated previously, the building-specific methodology of damage simulation implemented in FEMA P-58 is adopted. EDPs, such as peak story drift ratio (PSDR) and peak floor acceleration (PFA), from NRHAs create a dataset to estimate the probabilistic distribution parameters which are then used to simulate component damage states and resulting repair workload by Monte Carlo procedure. In this paper, damage simulation for structural components is generated from probabilistic distribution of local EDPs to capture the horizontal structural irregularity, whereas the nonstructural damage is simulated in terms of the average deformation on each story due to the relatively indeterminate layout of nonstructural components and mechanical equipment on the floor plan. To account for many uncertainties inherent in factors affecting component damage simulation, repair workload is calculated repeatedly for a large number (one thousand times) of realizations. Each realization represents one possible outcome of repair workload spatial distribution which provides detailed information on the type and the location of damaged component.

The repair time for a specific type of component at a specific floor is calculated by summing their respective repair workload ('worker-days') and dividing by the number of available workers assigned to that type of component on that floor. The repair time of components grouped into the same performance category is summed as the duration of the recovery subevent in Eq. (1). The precedent constraint that repairs of the components should be conducted in a realistic engineering order is also considered in this calculation with reference to the floor repair sequence defined in REDi<sup>TM</sup> Rating System [22]. It should be noted that all the subsequent repairs cannot initiate until the entire damaged structure is repaired due to the urgency of the structural integrity in safety issues. Based on that assumption, UTC repair duration on each floor is split into structural and nonstructural parts which are independently incorporated in the repair work schedule later.

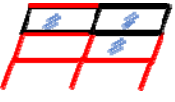
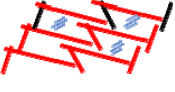
### 2.3 Work schedule arrangement

Recovery process is a set of pre-defined events arranged in chronological order. Work schedule is used to specify the sequence of these recovery activities as per the immediate post-hazard condition of the target building. In this method, building performance is classified as a limit state by the analytical result from probabilistic assessment on collapse, demolition, re-occupancy and serviceability of the studied building. Five limit states, which are mutually exclusive and exhaustive conditions, are introduced and listed in Table 1. The difference between each of them is the damage severity and the associated recovery work schedule. Additionally, recovery path is used to form a sequential bond between the overall state of building functionality and the implementation of work schedule. As shown in Table 1, to describe the progress of functionality restoration, recovery path comprises four distinct functional phases including non-occupied before repairs or replacement (*NOccBR*), non-occupied during repairs or replacement (*NOccDR*), occupied with loss of functionality (*OccLoss*) and occupied with full functionality (*OccFull*). The respective work schedule for each limit state herein is made on the consideration of the widely accepted engineering practice and the aforementioned functionality recovery subevent. Note that the activities can be conducted simultaneously if their alphabetical indices are in the same parenthesis in Table 1.

Table 1 – Building performance limit states

Limit States		Post-event Condition	Damage Severity	Recovery Path & Work Schedule			
LS <sub>1</sub>		Safe to occupy and fully functional.	Minor damage, and instant reuse without repairs.	<i>NOccBR</i>		<i>OccFull</i>	
				a		/	
LS <sub>2</sub>		Safely occupied, but partially malfunctional	Moderate damage that causes functionality loss.	<i>NOccBR</i>	<i>OccLoss</i>		<i>OccFull</i>
				a-(b,c-d,e)	-f-(g,h,i)		/
LS <sub>3</sub>		Reparable, but unsafe placard posted.	Extensive damage that triggers unsafe placard.	<i>NOccBR</i>	<i>NOccDR</i>	<i>OccLoss</i>	<i>OccFull</i>
				a-(b,c-d,e)	-f-g	-(h,i)	/



LS <sub>4</sub>		Irreparable, and need to be demolished.	Excessive residual deformation.	<i>NOccBR</i>	<i>NOccDR</i>	<i>OccFull</i>
				a-(b,c-d,e)	-j	/
LS <sub>5</sub>		Collapsed.	Loss of structural integrity.	<i>NOccBR</i>	<i>NOccDR</i>	<i>OccFull</i>
				(b,c-d,e)	-j	/

Note: a: Complete inspections; b: Secure financing; c: Conduct engineering review for design drawings; d: Obtain permit; e: Mobilize contractor; f: Complete repairs for structural UTC; g: Complete repairs for nonstructural UTC; h: Complete repairs for CNC; i: Complete repairs for VME, j: Complete reconstruction.

## 2.4 Stochastic modeling for recovery process

Due to the uncertainties in hazard intensity, post-event building performance and the subsequent recovery activities, the duration of story functionality restoration event,  $S_i$ , is modeled as a stochastic random process. The subscript indicates the number of the stories on which the pre-hazard functionality has been restored. Since  $S_1, S_2, \dots, S_n$  represent the time at which the repeating phenomenon of occurrence of functionality restoration, these random variables are referred to as arrival epochs, and form an arrival process which is a sequence of non-decreasing random variables [23],  $0 < S_1 \leq S_2 \leq \dots \leq S_n$ . For collapse (LS<sub>5</sub>) and demolition (LS<sub>4</sub>), the functionality restoration arrivals at all floor levels occur simultaneously at the time when building reconstruction completes. Besides,  $S_1, S_2, \dots, S_n$  can be equal to the same time spent in the post-earthquake inspection for the situation of instant reuse (LS<sub>1</sub>). In these cases, simultaneous arrivals ( $S_1=S_2=\dots=S_n$ ) definitely occur. Conversely, when *OccLoss* phase exists in the recovery path (e.g., LS<sub>2</sub> and LS<sub>3</sub>),  $S_i$  is a typical arrival process with a non-negative random increment. Hence, the time-dependent functionality recovery process specified by  $S_i$  is herein conceptualized as a state-based arrival process (SBAP).

The recovery arrival ( $X_j$ ), denoted as the time of building functionality restored on the  $j^{\text{th}}$  story, are used to calculate the arrival epoch series ( $S_i$ ). For example, let  $X_B, X_1, \dots, X_n$  be a time series representing the end of the functionality recovery events from the basement ( $X_B$ ) to the top floor ( $X_n$ ). The arrival epochs can be determined by Eq. (2), and  $S_i$  is the  $i^{\text{th}}$  order statistic of the recovery arrival series (Eq. (3)).

$$\{S_1, S_2, \dots, S_i, S_{i+1}, \dots, S_n\} = \text{Sort}(\{X_B, X_1, \dots, X_j, \dots, X_n\}), \text{ such that } S_i < S_{i+1} \quad (2)$$

$$S_i = \{X_B, X_1, \dots, X_j, \dots, X_n\}_{(i)} \quad (3)$$

It should be noted that the subscript of  $X_j$  indicates the location where the recovery event occurs, whereas the subscript of the arrival epochs ( $S_i$ ) refers to the number of restored stories which can be also interpreted as the order of the recovery arrivals. To visualize the determination procedure of the recovery arrivals across all the floors, Gantt chart is employed in the illustration of the recovery process and the workflow dependency among it (Fig.3). Off-site disruption caused by the post-hazard loss of OFS is depicted as  $\tilde{T}_{\text{OFS}}$  on the timeline denoting the longest time needed in the utility restoration of electricity, water and gas. Moreover, several preparatory activities (PA) (e.g., inspection, engineering review, etc.) should be conducted before the on-site repairs start. The time consumed in these activities is scheduled and shown in the *NOccBR* functional phase in Fig.3. For LS<sub>2</sub> and LS<sub>3</sub>, the structural UTC repairs are performed first from the bottom by all the workers available at the construction site.  $\tilde{T}_{\text{Str}}^{\text{all}}$  is time point defined as the end of all the structural repairs along the building height. After that, repairs for nonstructural UTC, CNC and VME can be scheduled in parallel and start simultaneously if the resourcefulness constraints (i.e., the number of workers available to work on a specific type of component and the total number of on-site workers) are obeyed. However, for limit states without *OccLoss* phase (i.e., LS<sub>1</sub>, LS<sub>4</sub> and LS<sub>5</sub>), recovery arrivals are directly equal to a same value, the end of inspection or reconstruction. As such, for a specific (e.g.,  $j^{\text{th}}$ ) story,  $X_j$  can be calculated by Eq. (4) given various limit states.



$$X_j | LS_k = \begin{cases} \max(\tilde{T}_{OFS}, \tilde{T}_{insp}), & k = 1 \\ \max(\tilde{T}_{OFS}, \tilde{T}_{VME}, \tilde{T}_{UTC}^j, \tilde{T}_{CNC}^j), & k = 2 \\ \max(\tilde{T}_{OFS}, \tilde{T}_{VME}, \tilde{T}_{UTC}^{all}, \tilde{T}_{CNC}^j), & k = 3 \\ \max(\tilde{T}_{OFS}, \tilde{T}_{rec}), & k = 4, 5 \end{cases} \quad (4)$$

where  $\tilde{T}_{insp}$  and  $\tilde{T}_{rec}$  are the end time of inspection and building reconstruction respectively.  $\tilde{T}_{UTC}^{all}$  indicates the end of UTC repairs among all the floors, and  $\tilde{T}_{VME}$  is the time that the VME repairs are all complete.  $\tilde{T}_{UTC}^j$  and  $\tilde{T}_{CNC}^j$  are the finishing time of UTC repairs and CNC repairs on the  $j^{th}$  story respectively. It is worth noting that workflow schedule of nonstructural UTC, CNC and VME repairs within a floor or across floors can be arranged in a variety of ways and have a great impact on the recovery arrivals on different stories for  $LS_2$  and  $LS_3$ . To minimize the uncertainty of recovery arrival estimation caused by workflow schedule, genetic algorithm using hierarchical non-dominated sorting (HNDS) [24] is employed to perform a multi-objective optimization and determine the optimal workflow schedule which achieves the minimum overall functionality disruption, the shortest recovery time and the highest labor efficiency. The recovery arrivals in later case study are calculated on this optimal workflow schedule for each realization.

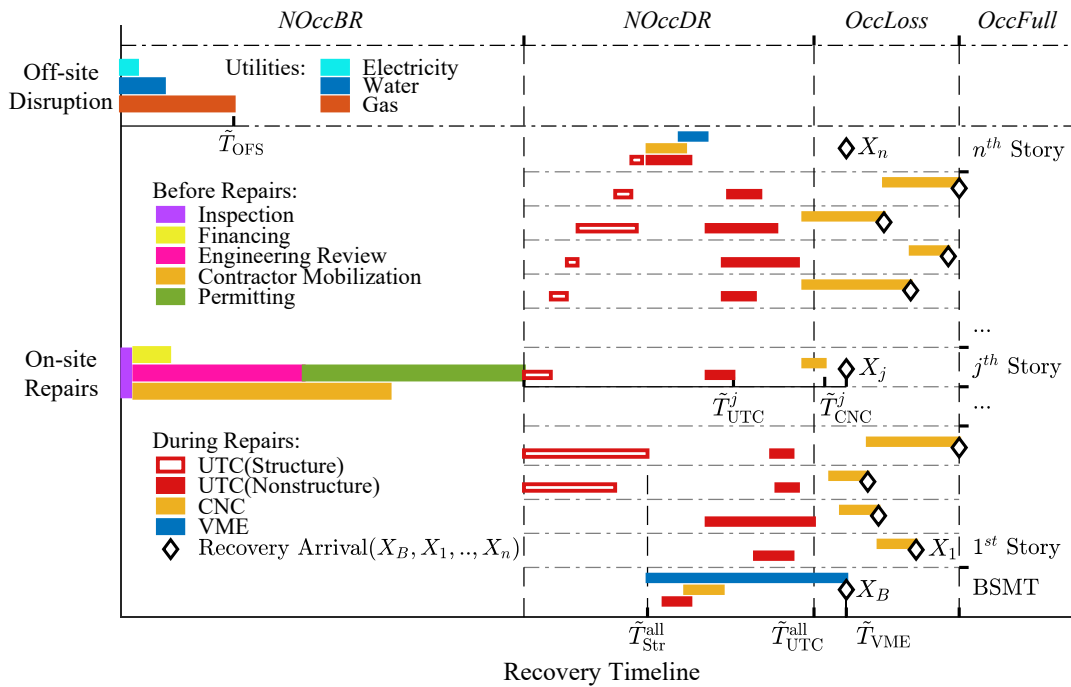


Fig. 3 – Gantt chart for recovery process

As a typical arrival process, the  $i^{th}$  arrival epoch,  $S_i$ , and the number of arrivals up to and including time  $t$ ,  $N(t)$ , are related by Eq. (4). The fact that these two events are logically equivalent.

$$\{N(t) \geq i\} = \{S_i \leq t\}, \text{ when } i > 0 \quad (4)$$

Where  $\{S_i \leq t\}$  is the event that the  $i^{th}$  arrival epoch occurs before time  $t$ , and  $\{N(t) \geq i\}$  implies the event that the number of arrivals by time  $t$ ,  $N(t)$ , must be at least  $i$ . In this principle, the complementary distribution function of the counting variables can be specified in terms of the distribution function of arrival epochs. The probability mass function of the counting process can be derived from the following equations:

$$\begin{aligned} \Pr\{N(t) = i | LS_k\} &= \Pr\{N(t) \geq i | LS_k\} - \Pr\{N(t) \geq i+1 | LS_k\} \\ &= \Pr\{S_i \leq t | LS_k\} - \Pr\{S_{i+1} \leq t | LS_k\} \end{aligned}, \text{ when } n > i > 0 \quad (5)$$



$$\Pr\{N(t) = i | LS_k\} = \Pr\{N(t) = n | LS_k\} = \Pr\{S_n \leq t | LS_k\} \quad , \text{ when } i = n \quad (6)$$

The counting process  $\{N(t); t > 0\}$  of the arrivals is used to quantitatively delineate post-earthquake building functionality restoration over time and stochastically model the recovery process. The time-dependent functionality is computed accounting the likelihood of the building being in each of the five limit states for a given ground-shaking intensity (Eq. (7)).

$$E[N(t)|IM] = \sum_{k=1}^5 \sum_i^{\Omega_k} i \times \Pr\{N(t) = i | LS_k\} \times \Pr\{LS_k | IM\} = \sum_i^n i \times \Pr\{N(t) = i | IM\} \quad (7)$$

Where  $E[N(t)|IM]$  is the expected time-dependent functionality given a certain ground motion intensity  $IM$ , measured in individual functionality unit which is ‘story’ herein.  $\Pr\{N(t) = i | LS_k\}$  is the probability mass function of the counting process by time  $t$  given  $LS_k$ .  $\Omega_k$ , denoted as the sample space of the number of arrivals for  $LS_k$  is  $\{0, 1, 2, \dots, n\}$  for  $LS_2$  and  $LS_3$ , and  $\{0, n\}$  for  $LS_1$ ,  $LS_4$  and  $LS_5$ .  $\Pr\{LS_k | IM\}$  is the probability that post-earthquake performance is in  $k^{\text{th}}$  limit state given ground motion intensity,  $IM$ .

### 3. Study case: a 40-story office building

The proposed assessment framework is implemented in a study case to model the post-earthquake recovery process of a typical tall commercial building. The archetype model is a 40-story steel moment-resisting frame (MF) office building with three basement levels. The structural configuration is a space frame using wide flange beams, built-up box columns, and welded beam-column connections. The floor plan and the isometric are illustrated in fig. 4, and Table 2 lists a summary of the section sizes of the steel MF.

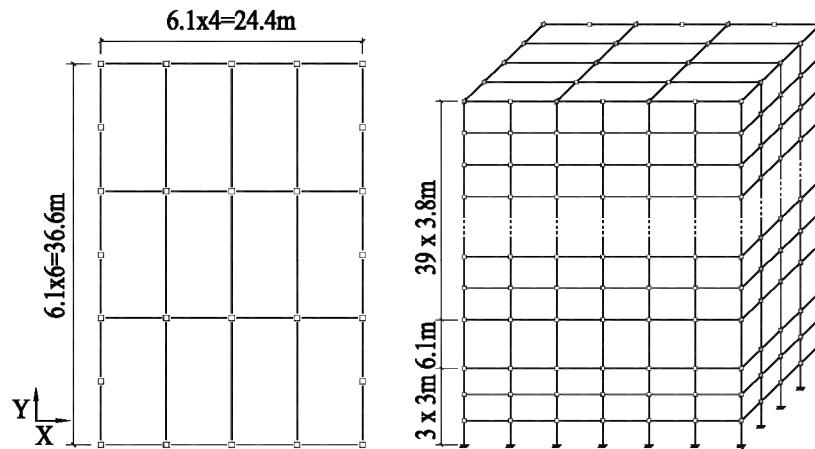


Fig. 4 – Prototype floor plan and isometric

Table 2 – Structural member section sizes

Level range	Wide flange beams			Box columns (in.)		
	Exterior	Interior short	Interior long	Interior	Exterior X	Exterior Y
Base to 10	W36×256	W36×282	W30×124	22×22(3)	26×26(3)	20×20(2.5)
11-20	W33×169	W36×194	W27×84	20×20(2)	26×26(2.5)	20×20(2)
21-30	W33×118	W33×169	W27×84	18×18(1)	24×24(1.5)	18×18(1)
31 to Roof	W24×62	W27×84	W24×76	18×18(0.75)	24×24(3)	18×18(0.75)

Note: 1 in. = 25.4mm, the number in parenthesis is the wall thickness of the box columns.

NRHAs are performed on a three-dimensional model of the prototype using *OpenSees*. Utilizing lumped plasticity modeling method, columns are modeled as elastic beam-column element with nonlinear fiber section hinges at two ends to capture the interaction between biaxial bending moment and axial force.



Modified Ibarra-Krawinkler (MIK) deterioration is adopted to predict the nonlinear behavior of the plastic hinge. Wide-flange beams in moment frames are modeled as elastic beam-column elements with plastic springs using MIK materials. Panel zones are modeled as an eight-element hinged parallelogram with a nonlinear rotational spring to represent shear nonlinear distortions, which is assumed to include a trilinear backbone without stiffness and strength deterioration. Column splices are erected using Partial Joint Penetration (PJP) welds, typically located 1.2m above the floor level every three floor. Fiber section plastic hinge like the ones at column ends are employed to model the column splices with an allowable tension strain limitation to account for the rupture of PJP welds at spliced zone.

The 22 pairs of bi-directional far-field ground motions provided in FEMA P695 [25] are selected to carry out incremental dynamic analysis (IDA). Since the prototype is asymmetric in plan, the ground motion pairs are applied in different orthogonal directions, which indicates there are 44 sets of NRHA results in total. The FEMA P695 scaling method is used in terms of normalized geometric-mean spectral intensity of the ground motion pairs with an adjustment to account for the effect of spectral shape. The surface ground condition is assumed as Site Class D in ASCE 7-16 [26], and the soil-structural interaction is ignored. The archetype building has a fundamental period of approximately 6s as per ASCE 7-16, and the maximum considered earthquake (MCE) response spectral acceleration for 2% in 50-year hazard is approximately 0.15g at the fundamental period. Scaling for IDA is conducted such that median spectral acceleration of the record set matched the targeted intensity levels, which ranges from 2% to 200%  $S_a$  of MCE. Fig. 5 illustrates the anchoring of median spectrum of record set to MCE spectral acceleration at the fundamental period and the range of scaling. Collapse fragility curve is developed from the results of IDA and used to simulate the occurrence of  $LS_5$  for each realization. While collapse is not evident, the maximum residual story drift ratio (RSDR) along the building height will be sampled as per the probabilistic distribution estimated from the results of NRHAs. If it exceeds the pre-defined threshold value 1%,  $LS_4$  would be assigned. Otherwise, building performance limit state is determined according to the component damage severity simulated from EDP distributions.

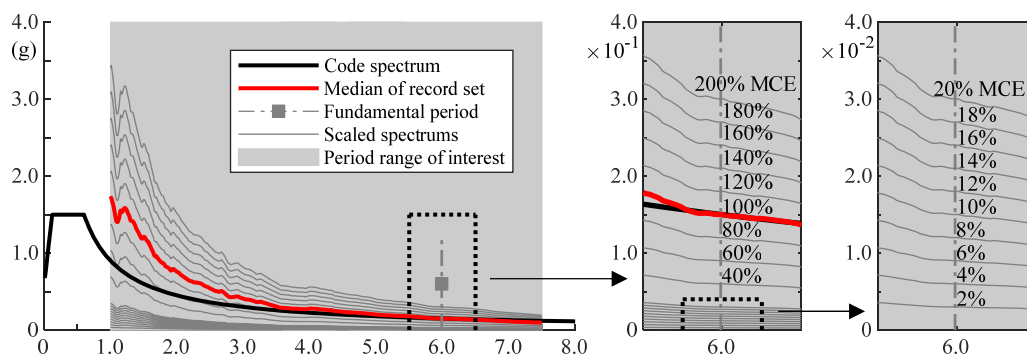


Fig. 5 – Anchoring of median spectrum of the record set to  $S_a$  of MCE and the scaling range

Table 3 summarizes components and equipment encompassed in the system reliability model of the archetype building, including the fragility identity, performance category, EDP, quantities in total, unit and location distribution. The column of fragility identities is excerpted from *PACT* [27], and those shaded in gray are structural components. The location distribution and quantities estimates are based on Normative Quantity Estimation Tool [27] and common commercial building configuration instead of the specific stock of the entire existing building. Component fragility function and respective consequence function are selected from FEMA P-58 to simulate damage states and calculate the associated repair workload.

Table 3 – Components encompassed in the system reliability model

Fragility ID	PC	EDP	Quantity	Unit	Location Distribution
B1031.001	UTC	PSDR	3096	1 EA	All the floors
B1031.011c	UTC	PSDR	26	1 EA	B3
B1031.021b	UTC	PSDR	112	1 EA	21,24,27,30,33,36,39





B1031.021c	UTC	PSDR	226	1 EA	B1,3,6,9,12,15,18,21,24,27,30,33,36,39
B1035.041	UTC	PSDR	456	1 EA	31-40
B1035.042	UTC	PSDR	318	1 EA	B3-B1, 1-30
B1035.051	UTC	PSDR	1552	1 EA	31-40
B1035.052	UTC	PSDR	856	1 EA	B3-B1,1-30
C2011.011b	UTC	PSDR	43	1 EA	All the floors
C3032.001b	UTC	PFA	547	600 ft <sup>2</sup>	All the floors
D4011.021a	UTC	PFA	83	1000 ft	All the floors
D4011.031a	UTC	PFA	37	100 EA	All the floors
B2022.202	CNC	PSDR	6933	30 ft <sup>2</sup>	1-40
C1011.001a	CNC	PSDR	365	100 ft	All the floors
C3034.001	CNC	PFA	6192	1 EA	All the floors
D2021.011a	CNC	PFA	6	1000 ft	All the floors
D2022.011a	CNC	PFA	37	1000 ft	All the floors
D2031.021a	CNC	PFA	24	1000 ft	All the floors
D3041.011a	CNC	PFA	31	1000 ft	All the floors
D3041.031a	CNC	PFA	3720	1 EA	All the floors
D3041.041a	CNC	PFA	2890	1 EA	All the floors
D5012.021a	CNC	PFA	43	1 EA	All the floors
D1014.011	VME	PFA	12	1 EA	B3, Roof
D3031.011c	VME	PFA	2	1 EA	20
D3031.021c	VME	PFA	2	1 EA	Roof
D3052.011d	VME	PFA	13	1 EA	20, Roof
D5012.013a	VME	PFA	17	1 EA	20

Note: The structural components are shaded in gray; EA = each; 1 ft = 0.3048 m; 1 ft<sup>2</sup> = 0.0929 m<sup>2</sup>

As noted earlier, the number of available workers is directly influential in calculating repair duration of each PC. Hence, repair labor size and allocation are imposed as the resourcefulness constraints on recovery process modeling. The numbers of available workers are assumed as 38 per floor (1 worker/250sf) for UTC and CNC, and 3 per damaged unit for VME. The total number of workers across multiple floors is set as 114 based on the maximum number of workers on site excerpted from REDi<sup>TM</sup> Rating System. Additionally, utility disruption times to water, gas and electrical systems, modeled as lognormal random variables, are also considered as off-site impediments on the on-site recovery. The 50% probability of non-exceedance values are set as 4 days (electricity), 21 days (water), and 42 days (gas), and the dispersions are 1.2, 0.6, and 1.1 respectively. Table 4 lists the probabilistic distribution parameters of time consumed in preparatory activities from [22], and the time for replacement of building is set as 1075 days (25 days/story).

Table 4 – Probabilistic distribution parameters of preparatory activities (data from [22])

Limit States	Inspection		Financing		Engineering Review		Contractor Mobilization		Permitting	
	$\theta$	$\beta$	$\theta$	$\beta$	$\theta$	$\beta$	$\theta$	$\beta$	$\theta$	$\beta$
LS <sub>1</sub>	1	0.54	-	-	-	-	-	-	-	-
LS <sub>2</sub>	1	0.54	7	0.5	14	0.3	21	0.7	7	0.86
LS <sub>3</sub>	1	0.54	7	0.5	28	0.5	49	0.35	56	0.32
LS <sub>4</sub>	5	0.54	7	0.5	294	0.45	49	0.35	56	0.32
LS <sub>5</sub>	-	-	7	0.5	294	0.45	49	0.35	56	0.32

Note:  $\theta$  denotes median;  $\beta$  denotes dispersion.

After generating 1000 realizations of component damage, residual drift demands and collapse intensity thresholds, the expected time-dependent functionality (TDF) in terms of the number of functional stories is computed using Eq. (7) for each ground motion intensity level. The resulting recovery curves across IM



levels are shown in Fig. 6. Normalized functionality is expressed by the color (from red to green as the functionality increases) of the recovery curve. It should be noted that each point on the curve indicates the expected value of the stochastic recovery process  $\{N(t)\}$  at time  $t$ . For example,  $\{N(t)\}$  on the 750th day of the recovery process at 40% MCE intensity level is a discrete random variable with probability mass function as shown in Fig. 6 (right-hand panel). At lower intensities, the expected functionality soars to the pre-hazard level immediately after the occurrence of hazard. This reveals that the component damage caused at lower intensities is relatively slight and the impacted building can achieve full function quickly on the optimal workflow schedule. On the other hand, the curve of expected functionality restores slowly with a period of delay at the beginning and a flat platform in the middle of the recovery process at intensity levels larger than 10% Sa of MCE. This observation can be partially attributed to that some severe damage happens to vital mechanical equipment and the functionality of the building can be restored only after the repairs of these facilities complete. Additionally, as the expected functionality is a probability-weighted average of functionality curves of various limit states, the full functionality time points of non-replacement limit states (i.e.,  $LS_1$ ,  $LS_2$ , and  $LS_3$ ) becomes partial functionality time points when the probability of demolition and collapse increases at higher intensities. This is the reason that the middle platform appears.

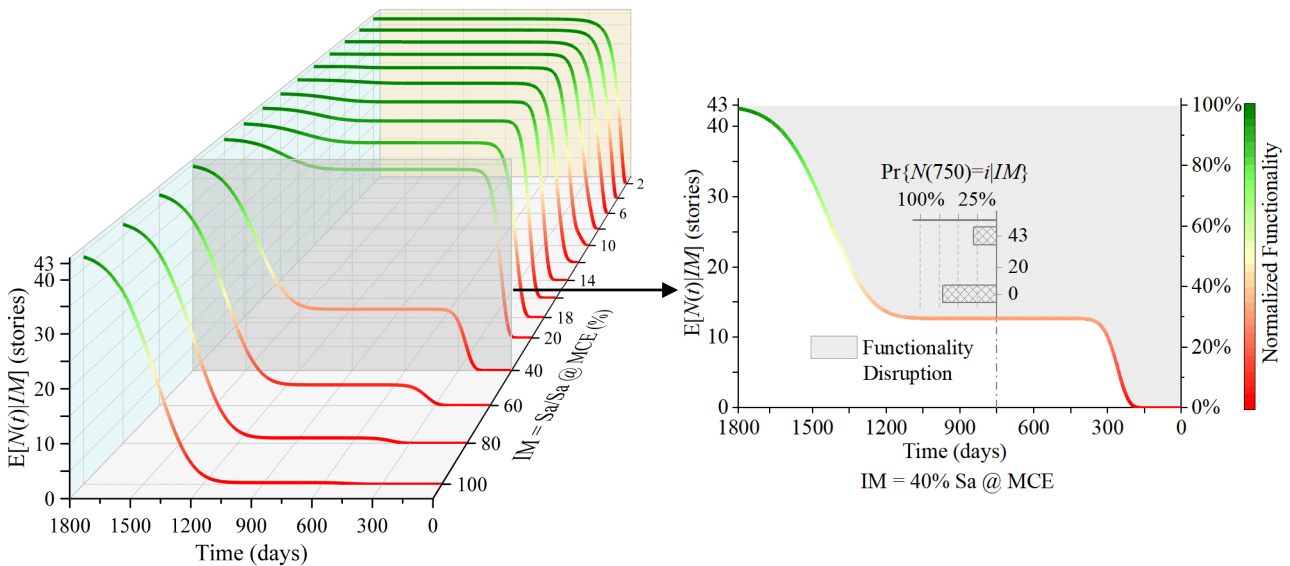


Fig. 6 – Expected time-dependent functionality recovery curves

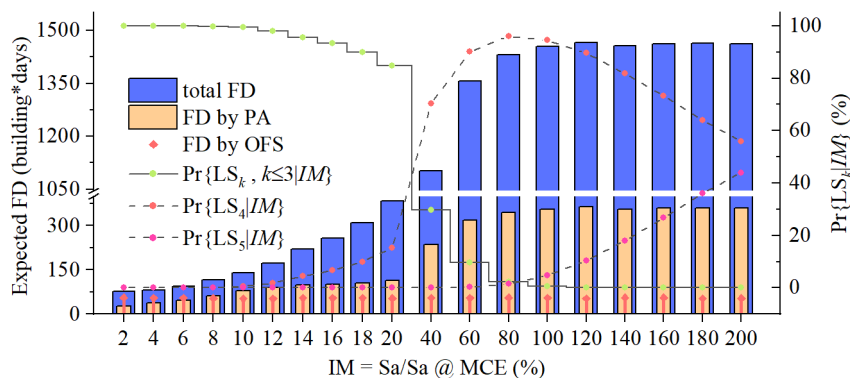


Fig. 7 – Expected functionality disruption and the probability of limit states across multiple intensity levels

Functionality loss informs the decline of the supposed economic income of CBD towers when it is multiplied by the profit that each functionality unit (story) can make on the pre-hazard condition. Hence, functionality disruption (FD) can be served as an ideal measure of resilience, since it establishes a direct connection between the cumulative impact of hazard damage during recovery period with the economic



concern of building owners. FD herein is defined as the shaded area between the time-dependent functionality curve and the horizontal line at full functionality as shown in Fig. 6, and the Fig. 7 illustrates the expected FD across all the intensity levels considered in the study case. At lower intensities, it is observed that the total FD increases slowly and is dominated by the proportion of FD caused by OFS failure when IM is less than 10% MCE level. This points out that loss of utility service outweighs preparative and repair activities in the influence of building resilience at extra-low intensities. In Fig. 7, there is a significant nonlinear increase in total FD when the intensity level exceeds 20% spectral acceleration of MCE. This dramatic variation can be explained by the fact that the probability of non-exceedance of LS<sub>3</sub> drops sharply to 29% and disruption period gets close to the sum of the time consumed in PA and the time for building replacement as discussed previously. It should be noted that limited to relative scarcity of prior relevant study as to tall buildings, the resulting probability of LS<sub>4</sub> given IM can vary substantially as different irreparable EDP threshold is chosen in the simulation. Thus, the intensity level that FD starts to increase nonlinearly (i.e., 40% MCE level in Fig. 7) can become larger when the maximum allowable RSDR for reparability increases. However, due to the limited collapse capacity of the building, this value cannot exceed the median collapse ground motion intensity level.

#### 4. Conclusion

The primary motivation and contribution of this study is to develop a resilience-based probabilistic framework for assessing the time-dependent functionality of tall buildings through the post-earthquake recovery modeling. The recovery process in this methodology is stochastically modeled under the labor force constraint, and it integrates component-level damage, building-level post-event performance and story-level functionality restoration. As a building-specific SSB method, the framework provides an insight into the variation of functionality disruption across multiple intensity levels incorporating off-site impediment and preparative activities for repairs or reconstruction. Additionally, the framework presented in this paper can be also used to facilitate the decision-making for the improvement of resilience-based performance in future study and guide the design practices to meet the resilience-based objectives.

#### 5. Acknowledgements

The authors acknowledge support from National Natural Science Foundation of China under Grant No. 51638012 and National Science Foundation Award of America No. 1538866.

#### 6. Copyrights

17WCEE-IAEE 2020 reserves the copyright for the published proceedings.

#### 7. References

- [1] Koduru SD, Haukaas T (2009): Probabilistic seismic loss assessment of a Vancouver high-rise building. *Journal of Structural Engineering*, **136**(3), 235-245.
- [2] Hutt CM, Almufti I, Willford M, Deierlein GG (2015): Seismic loss and downtime assessment of existing tall steel-frame buildings and strategies for increased resilience. *Journal of Structural Engineering*, **142**(8), C4015005.
- [3] Zeng X, Lu X, Yang T, Xu Z (2016): Application of the FEMA-P58 methodology for regional earthquake loss prediction. *Natural Hazards*, **83**(1), 177-192.
- [4] Wang S, Lai JW, Schoettler MJ, Mahin SA (2017): Seismic assessment of existing tall buildings: A case study of a 35-story steel building with pre-Northridge connection. *Engineering Structures*, **141**, 624-633.
- [5] Guan X, Burton HV, Moradi S (2018): Seismic performance of self-centering steel moment frame building: From component-level modeling to economic loss assessment. *Journal of Constructional Steel Research*, **150**, 129-140.



- [6] Zhang P, Peeta S (2011): A generalized modeling framework to analyze interdependencies among infrastructure system. *Transportation Research Part B: Methodological*, **45**(3), 553-579.
- [7] Guidotti R, Chmielewski H, Unnikrishnan V, Gardoni P, McAllister T, Van de Lindt J (2016): Modeling the resilience of critical infrastructure: The role of network dependencies. *Sustainable and resilient infrastructure*, **1**(3-4), 153-168.
- [8] Burton HV, Kang H, Miles S, Nejat A, Yi Z (2019): A framework and case study for integrating household decision-making into post-earthquake recovery models. *International Journal of Disaster Risk Reduction*, **37**, 101167.
- [9] Kang H, Yi Z, Burton HV (2019): Effect of the Los Angeles Soft-Story Ordinance on the post-earthquake housing recovery of impacted residential communities. *Natural Hazards*, **99**, 161-188.
- [10] ASCE (2019): Resilience-based performance: Next generation guidelines for buildings and lifeline standards. Reston, VA, USA.
- [11] Isumi M, Nomura N, Shibuya T (1985): Simulation of post-earthquake restoration of lifeline systems. *International journal of mass emergencies and disasters*, **3**(1), 87-105.
- [12] Nojima N, Kameda H (1992): Optimal strategy by use of tree structure for post-earthquake restoration of lifeline network systems. *Proceedings of the 10<sup>th</sup> World Conference on Earthquake Engineering*, 5541-5546.
- [13] Chang SE, Shinozuka M (2004): Measuring improvements in the disaster resilience of communities. *Earthquake Spectra*, **20**(3), 739-755.
- [14] Miles SB, Burton HV, Kang H (2019): Community of practice for modeling disaster recovery. *Natural Hazards Review*, **20**(1), 04018023.
- [15] Miles SB, Chang SE (2006): Modeling community recovery from earthquakes. *Earthquake Spectra*, **22**(2), 439-458.
- [16] Miles SB, Chang SE (2011): ResilUS: A community based disaster resilience model. *Cartography and Geographic Information Science*, **38**(1), 36-51.
- [17] Burton HV, Deierlein GG, Lallemand D, Lin T (2015): Framework for incorporating probabilistic building performance in the assessment of community seismic resilience. *Journal of Structural Engineering*, **142**(8), C4015007.
- [18] Zhang W, Lin P, Wang N, Nicholson C, Xue X (2018): Probabilistic prediction of postdisaster functionality loss of community building portfolios considering utility disruptions. *Journal of Structural Engineering*, **144**(4), 04018015.
- [19] Mitrani-Resier J, Wu S, Beck JL (2016): Virtual Inspector and its application to immediate pre-event and post-event earthquake loss and safety assessment of buildings. *Natural Hazards*, **83**(3), 1861-1878.
- [20] FEMA P-58-1 (2012): Seismic Performance Assessment of Buildings Volume 1: Methodology. *Applied Technology Council*, Redwood City, CA, USA.
- [21] FEMA P-58-2 (2012): Seismic Performance Assessment of Buildings Volume 2: Implementation Guide. *Applied Technology Council*, Redwood City, CA, USA.
- [22] Almufti I, Willford M. (2013). Resilience-based earthquake design (REDi) rating system, version 1.0. *Arup Group, London, United Kingdom*.
- [23] Gallager R. *6.262 Discrete Stochastic Processes*. Spring 2011. Massachusetts Institute of Technology: MIT OpenCourseWare, <https://ocw.mit.edu>. License: Creative Commons BY-NC-SA.
- [24] Bao C, Xu L, Goodman ED, Cao L. (2017): A novel non-dominated sorting algorithm for evolutionary multi-objective optimization. *Journal of Computational Science*, **23**, 31-43.
- [25] FEMA P695 (2009): Quantification of Building Seismic Performance Factors. *Applied Technology Council*, Redwood City, CA, USA.
- [26] ASCE 7-16 (2016): Minimum Design Loads and Associated Criteria for Buildings and Other Structures. *ASCE/Structural Engineering Institute (SEI)*, Reston, VA, USA.
- [27] FEMA PACT (2018): Performance Associated Calculation Tool "Version 3.1.1". *Applied Technology Council*, Redwood City, CA, USA.